Nigerian Research Journal of Chemical Sciences (ISSN: 2682-6054)
Volume 12, Issue 1, 2024

Synthesis and Characterization of *Cola acuminata* Dye Nanoparticle for Corrosion Inhibition of Mild Steel in 1 M HCl Solution

*[1,2]Omogbehin Samson Adehuga, [1]Olasehinde Emmanuel Folorunsho, [1]Adebayo Matthew Ayorinde,
[1]Jamiu Mosebolatan Jabar
[1] Department of Chemistry, The Federal University of Technology, Akure, Ondo State, Nigeria
[2] Department of Science Laboratory Technology, Federal Polytechnic, Ile Oluji, Ondo State, Nigeria
* Corresponding author: adehugasamson@gmail.com; samomogbehin@fedpolel.edu.ng

Accepted: April 24, 2024. Published Online: May 7, 2024

ABSTRACT

This study investigated a new environmentally friendly method for protecting mild steel from corrosion in acidic environments. This was done by synthesizing and testing dye nanoparticles made from an extract of *Cola acuminata* (kola nut seeds) as a potential alternative to current synthetic and inorganic anti-corrosion additives used in industrial cleaning and pickling operations. The dye extract was obtained by dissolving 1 kg of the *Cola acuminata* seed powder into 2 L of 50% ethanol. The filtered extract (10 ml) was added to 90 ml of 1mM $AgNO_3$ solution, homogenized and centrifuged to synthesize the nanoparticles. The dye extract was characterized using qualitative phytochemical analysis, UV/Visible spectrophotometer and Fourier Transform IR (FTIR) while the nanoparticles were characterized using UV/Visible spectrophotometer, FTIR, XRD, SEM-EDX, and N_2 adsorption/desorption analysis. Analysis revealed that *Cola acuminata* dye exhibited light absorption properties characteristic of a dye molecule, The silver nanoparticles were crystalline, oval/spherical, and containing hydroxyl, carbonyl, amine, and alkene groups. Adding *Cola acuminata* dye or nanoparticles decreased mild steel corrosion rate while acting as an endothermic, surface-adsorbing inhibitor. The *Cola acuminata* nanoparticles exhibited superior inhibition efficiency compared to the crude *Cola acuminata dye* extract. Therefore, *Cola acuminata* nanoparticles can be used as an ecofriendly corrosion inhibitors in acidic medium.

Keywords: Corrosion, silver nanoparticles, *Cola acuminata*, mild steel

INTRODUCTION

Mild steel is among the most versatile engineering materials used in structural applications. They are used, among other things, as vital components of machinery, building construction, bridge trusses, screws, military weaponry, and automobile parts. These materials are attractive due to their ease of use, excellent mechanical properties, and ease of production [1]. Mild steel, also known as plain-carbon steel is inexpensive and has good properties that allow it to be used for a variety of applications, making the steel vulnerable to corrosion attack.

One of the most effective ways to stop corrosion damage is to use corrosion inhibitors [2]. Corrosion inhibitor is one that, when introduced in small amount to a given environment, slows down the rate at which metals exposed to it corrode. The inhibitors alter the kinetics of the electrochemical events that comprise the corrosion process by delaying the cathodic reduction reaction or the rate at which metal dissolves in the corrosive fluid. Corrosion inhibitors change the structure of the electrical double layer. by adsorbing on the metal surface. The bulk of effective inhibitors used in industry are organic compounds with oxygen, sulfur, nitrogn atoms, π-bonds, and/or aromatic ring(s) [3]. Organic dyes are compounds with promising properties for preventing corrosion. Their coloration is caused by heteroatoms and π-electron systems, which also suggest that they have a great propensity to adsorb on metal surfaces and other adsorbents [3].

Nanomaterials have attracted a lot of attention in both science and corrosion prevention due to their increased surface area for a faster reaction time as well as their ability to form self-assembling coatings on metal surfaces [4]. Silver nanoparticles can prevent corrosion on metal surfaces by promoting the growth of a protective layer [1].

Cola acuminata (CA) has been the subject of intensive phytochemical study and chemical component isolations. These studies have revealed the presence of several groups, including tannins, alkaloids, flavonoids, anthraquinones, which contain atoms like O and N and functional groups that can help corrosion inhibition [5]. *Cola acuminata* extract has been studied for its potential to prevent mild steel corrosion in acidic conditions [6] and even employed to synthesize *Cola acuminata* silver nanoparticles (CA AgNPs) as a stabilizer [7]. Information regarding the use of CA AgNPs dye as corrosion inhibitors specifically remains scarce.

The aim of this study is to synthesis and characterize CAAgNPs dye for corrosion Inhibition on mild steel in 1 M HCl. The objectives are to extract a natural dye from Cola *acuminate seed;* synthesize its silver nanoparticles and compare their corrosion inhibition efficiency on mild steel in 1 M HCl.

MATERIALS AND METHODS

Preparation and characterization of dye extract and silver nanoparticles of *Cola acuminate* (CA AgNP)

The seeds of *Cola acuminata* were cleaned to remove any contaminants. They were ground to powder, sieved, and stored in an airtight container for 21 days. 2 L of 50% ethanol was used to dissolve 1 kg of the ground sample and kept for 3 days. 10 ml of extract and 90 ml of 1mM $AgNO_3$ solution, were combined, and the mixture was homogenized using a magnetic stirrer to produce a dark brown solution that indicated the presence of nanoparticles (NPs). After 30 minutes of centrifugation at 4000 rpm, the resultant solution settled. After a thorough washing in distilled water, the product was dried at 60 °C in an oven and kept in a desiccator [8].

Sample analysis

Phytochemical analysis of the CA dye extract was carried out following the reported methods [9-10]. UV/Visible analysis was carried out using UV/Visible spectrophotometer (Model Genesys 10 S), between 200 and 800 nm. Using Agilent Technologies FTIR spectroscopy, the functional groups in the dye and nanoparticles were detected at a resolution of 8 cm^{-1}, covering a scan range of 600 cm^{-1} to 4000 cm^{-1}. XRD (Model Rigaku Mini-flex II (Japan)) was used to determine the synthesized CA Ag NP's crystalline nature. The elemental components of the CA AgNP sample were examined using an EDX connected with a scanning electron microscope (Thermo Scientific). The N_2 adsorption-desorption analysis was performed using a TriStar II 3020 2.00 analyzer (Micromeritics Corp., USA). The specific surface area, particle size, and average pore diameter of the nanoparticles were estimated using the Barrett-Joyner-Halenda (BJH) adsorption model of Brunauer-Emmett-Teller (BET) analyser.

Corrosion inhibition studies

Preparation of mild steel

The investigation employed the following mild steel compositions: Fe=99.11, Mn=0.359, C=0.149, Cr =0.055, S=0.059, and Ni= 0.048. After being manually polished with silicon carbide paper and thoroughly washed with distilled water, acetone and ethanol were used to degrease the coupons, which were allowed to air dry in a desiccator. Using mild steel of dimension 22 mm x 18 mm x 2 mm coupons, the sample weights were obtained using an electronic weighing balance. The experiment employed double-distilled water, and each reagent used in the study was graded analytically [11].

Corrosive and inhibitor environments preparation

Diluting concentrated HCl (36.5%, analytical grade) with distilled water, 1.0 M HCl aqueous solution was prepared. A 1.0 M HCl solution was used to dissolve precisely weighed quantities of plant extract and silver nanoparticle to create inhibitor solutions with concentrations ranging from 0.2 to 1.2 g/L.

Weight-loss method

For three hours, pre-weighed mild steel coupons were submerged in 1.0 M HCl with and without varying concentrations of *Cola acuminata* crude dye and nanoparticles at 303–333 K. The coupons were taken out, submerged in a NaOH solution, cleaned with acetone and distilled water, dried, and weighed to determine the amount of weight loss. The studies were conducted in triplicate, and the computation was based on the average weight loss figures. This was used to determine the corrosion rate (C_R) in g cm^{-2} h^{-1} , percentage inhibition efficiency (*IE*%). And surface Coverage (ϴ). Equations (1),(2)and (3) were used to calculate the values of C_R, , % *IE* and ϴ respectively, as described by Olasehinde *et al* [11].

$$C.R = \frac{\Delta w}{At} \quad (1)$$

Where Δw = change in weight in g

A = Area in Cm^2

t = Time in hour

$$\% \, I.E = I - \frac{\Delta w_1}{\Delta w_2} \times 100 \quad (2)$$

Where Δw_1 and Δw_2 are weight loss in the absence and presence of inhibitor

$$\Theta = 1 - \frac{\Delta w_1}{\Delta w_2} \quad (3)$$

The procedure was repeated at temperature values of 313K, 323K and 323K.

Surface morphology

Using scanning electron microscopy (SEM) in vacuum at an operating potential of 15 kV, the surface morphology of mild steel coupons immersed in 1.0 M HCl solution in the presence and absence of different concentrations of CA crude dye and CA AgNP was investigated.

Energy Dispersive X-ray spectroscopy (EDX) was used to analyze the elemental composition of the surfaces.

RESULTS AND DISCUSSION

Using a visual inspection, the color change in the volumetric flask containing the $AgNO_3$ solution with CA extract was seen. The $AgNO_3$-extract solution's hue transitioned from pale brown to dark brown. The development of Ag nanoparticles in the solution is shown by this color shift [4]. The apparent hue shift supported the Ag^+ reduction. This shift in hue denotes the creation of Ag nanoparticles in the solution as a result of the silver nanoparticles' surface plasmon vibration being excited [4].

Phytochemical analysis

Cola acuminata dye extract's phytochemical examination reveals the following compounds: tannins, phenols, flavonoids, and alkaloids. Studies reveal that the majority of green inhibitors are made up mostly of phenols, tannins, and alkaloids [12].

Table 1: Phytochemical analysis of CA dye extract

Parameter	Observation
Alkaloids	+++
Flavonoids	++
Saponins	+
Tannins	++
Phenols	+++

UV-Vis spectroscopy

For the CA dye extract, two absorption peaks were seen at about 230 and 340 nm (Fig. 1a). Absorption around 230 and 340 nm indicates presence of aromatic chromophores (light absorption properties characteristic of a dye molecule) of some flavonoids and their derivatives. The identification of peaks 230 and 340 as flavonoids and their derivatives was based on their occurrence within the range of 230 to 400 nm, which is in line with the findings reported by Mabasa *et al*. [13]. The two absorption spectra for flavonoids and phenolic substances are caused by the presence of aromatic rings and other rings [14]. The CA AgNP observed UV-vis spectra are shown in Fig. 1b. According to reports, the absorbance values of silver nanoparticles produced via green synthesis are between 400 and 500 nm in the UV/visible range [15]. The absorption spectrum of CA AgNP has two distinct peaks, namely 238.6 and 407.8. The creation of AgNPs is responsible for the conspicuous peak in this study, which is at 407.8 nm. This result agrees with the findings of Tiara *et al* [16], who found that the strongest absorption peaks were at 400 nm, for the UV-VIS spectrum analysis for silver nanoparticles synthesized using *diospyros maritima* leaves eextract. The absorbance value obtained in this study is also close to the work of Ahmed *et al* [17] who obtained an absorbance value of 445 nm for the synthesis of AgNPs from *Azadirachta indica* aqueous leaf extract. This peak indicates the formation of AgNPs because it is within the range of the surface plasmon resonance (SPR) for AgNPs. The other peaks may be due to some component in the crude extract of *Cola acuminata.*

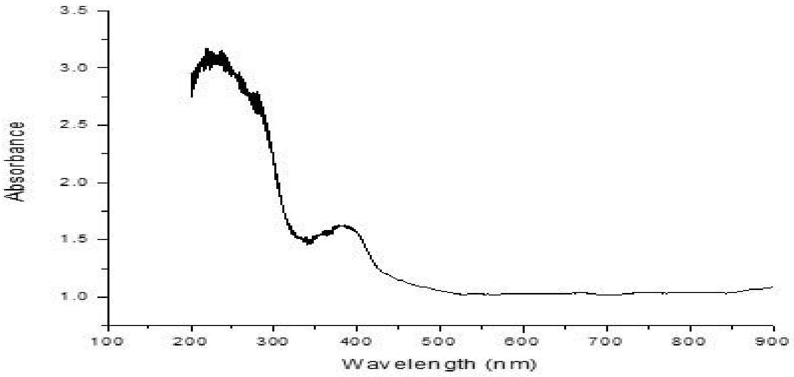

Fig 1 (a): UV–Vis absorption spectrum of CA dye

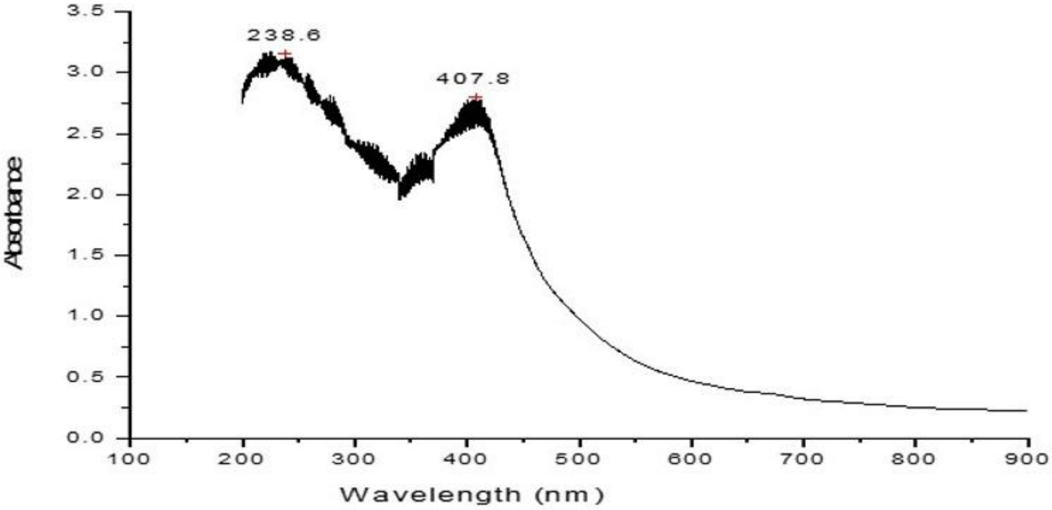

Fig 1 (b): UV–Vis absorption spectrum of CA AgNPs dye

FT-IR Analysis

The FT-IR spectra of the CA AgNP and the CA dye extract are shown in Figures 2a and 2b. The nanoparticles and dye extract have specific functional groups, as shown by the FTIR spectra, which span from 3294.96 cm^{-1} to 812.56 cm^{-1}. The absorption bands for the dye extract and artificial nanoparticles at between 3294.96 cm^{-1} and 3268.97 cm^{-1}. relate to the N-H stretching of an amine or the O-H stretching of alcohol. The nanoparticles' peak seems to have grown longer. According to Supraja *et al* [18], the C-H bending is indicated by the peak between 2929.68 cm^{-1} and 2855.14 cm^{-1}, whereas the stretching of the C=C or C=O vibrations is indicated by the peak between 1733.21 cm^{-1} and 1625.11 cm^{-1}. The dye and nanoparticles, according to these findings, comprise O–H, C=O, C=C, N- H and C–H) atoms in functional groups that satisfy the requirements of a typical corrosion inhibitors [19-21].

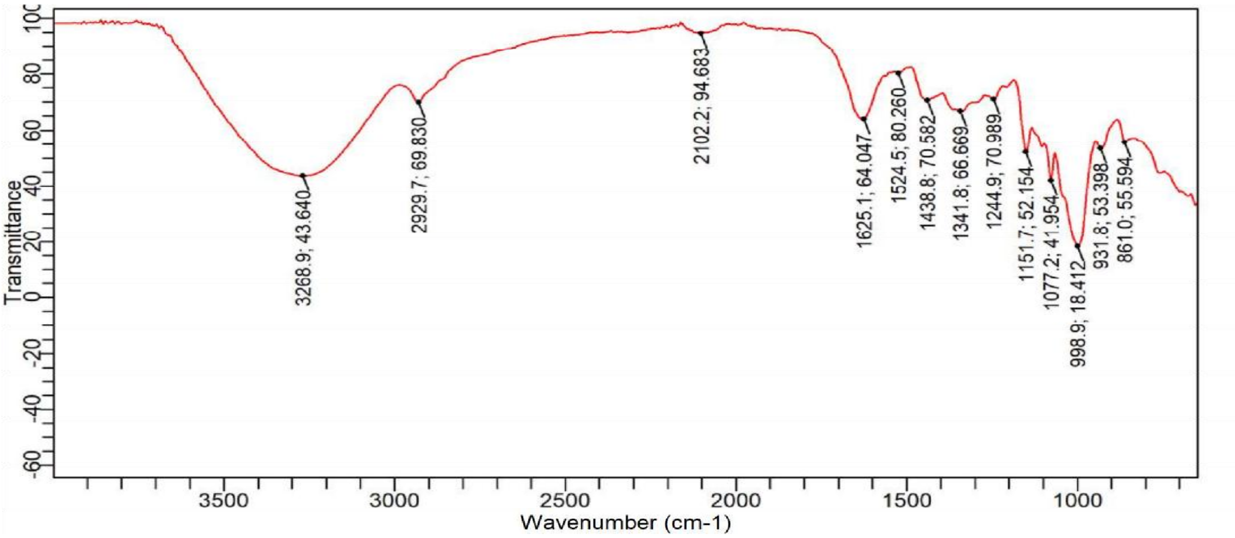

Fig 2(a): FTIR spectrum of CA dye

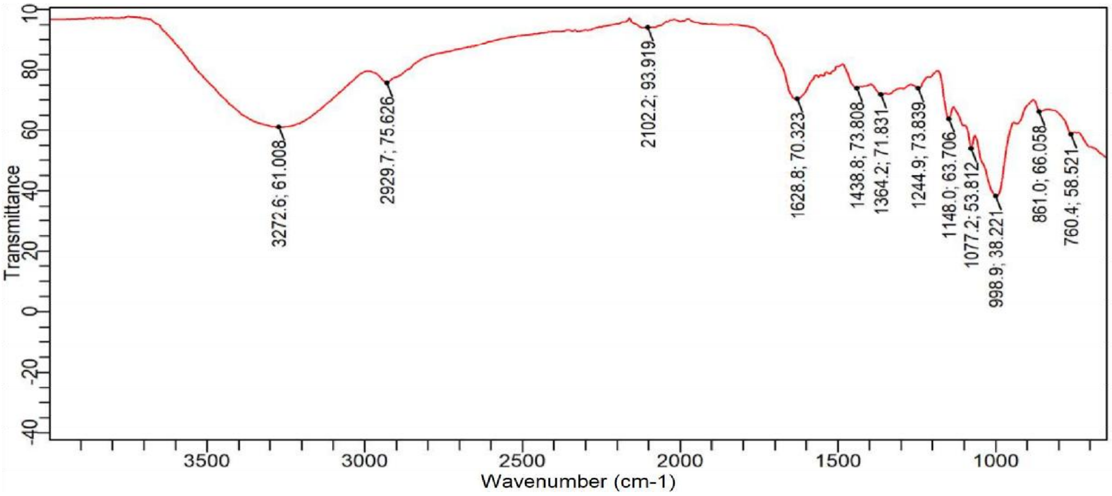

Fig 2(b): FTIR spectrum of CA AgNP

Scanning electron microscopy (SEM) coupled with Energy Dispersive X-ray (EDX) analysis

The particles were round and oval in shape, as shown by the SEM images. A small number of individual particles were also visible, although the majority of the nanoparticles were aggregated [22]. The elemental silver in the nanoparticles was verified by EDX analysis. The profiles of SEM-EDX are displayed in Figs. 3a and 3b.

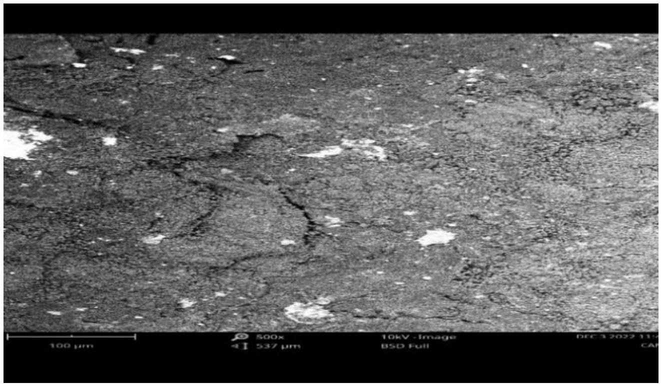

Fig 3(a): SEM micrographs of CA Ag NP

Element Number	Element Symbol	Element Name	Atomic Conc.	Weight Conc.
8	O	Oxygen	71.40	73.12
6	C	Carbon	17.75	13.65
7	N	Nitrogen	10.08	9.03
47	Ag	Silver	0.51	3.55
20	Ca	Calcium	0.25	0.64

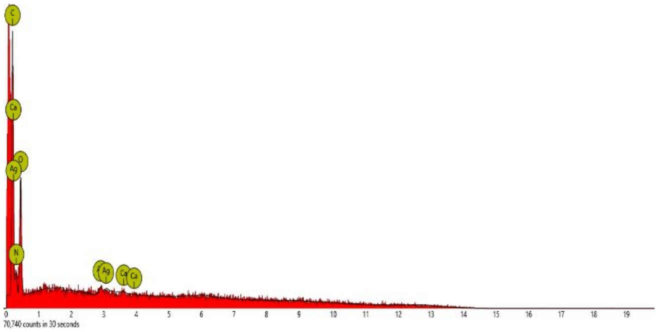

Fig 3(b): EDX Spectrum of CA AgNP

X-ray diffraction

The X-ray diffraction (XRD) pattern of the dried nanoparticles extracted from colloid samples further supports the crystalline nature of Ag nanoparticles. (Fig. 4). The X-ray diffraction pattern of the nanoparticles confirms the face-centered cubic (FCC) crystalline structure of silver.

Intense peaks at 2θ values of 10.52°, 20.310, 40.40°, and 62.32° corresponding to Bragg's reflection based on the (FCC) structure of the nanoparticles were shown by the XRD analysis. A distinct broadening of the XRD peaks suggests that the material that has been manufactured contains particles inside the nanoscale range. This demonstrates unequivocally that the crystalline silver nanoparticles produced by the CA's reduction of Ag+ ions to Ago [23].

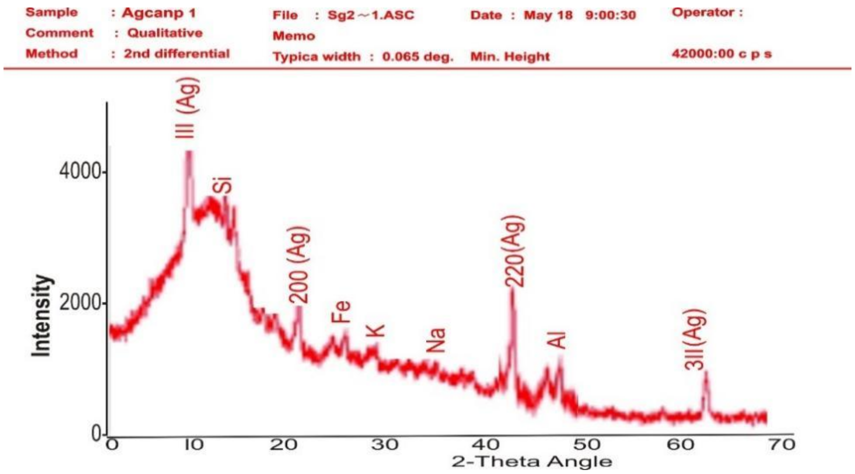

Sample : Agcanp 1
Comment : Qualitative
Method : 2nd differential
File : Sg2～1.ASC
Memo
Typica width : 0.065 deg.
Date : May 18 9:00:30
Min. Height
Operator :
42000:00 c p s

Fig 4: XRD Spectrum of CA AgNP

N_2 gas adsorption/desorption analysis

The particle sizes of CA AgNP were characterized by nitrogen gas adsorption/desorption analysis [24] The adsorption and desorption isotherms obtained from the analysis carried out for this study are displayed in Fig. 5(a). On the isotherm, the Type IV hysteresis loop—a sign of CA AgNP's mesoporous structure was plainly visible [25].

Assuming the specific surface area of the Ag nanoparticles is 20.12 m^2/g. The formula $D_{BET} = 6000/(\rho \cdot Sw)$ (in nm) can be used to determine the average equivalent particle size of a solid, spherical particle with a smooth surface and equal size. Here, ρ represents the theoretical density in g/cm^3, S_w denotes the measured surface area of the powder in m^2/g, and D_{BET} is the average diameter of a spherical particle. Based on the expression, the average particle size of CA AgNP was found to be 31.66 nm. The BJH isotherm for the CA AgNP differential pore size distribution curves is shown in Fig. 5(b). The calculated pore size volume of the nanocomposite for CA AgNP is 21.23 nm, ranging between 2 and 50 nm for mesoporous materials [24].

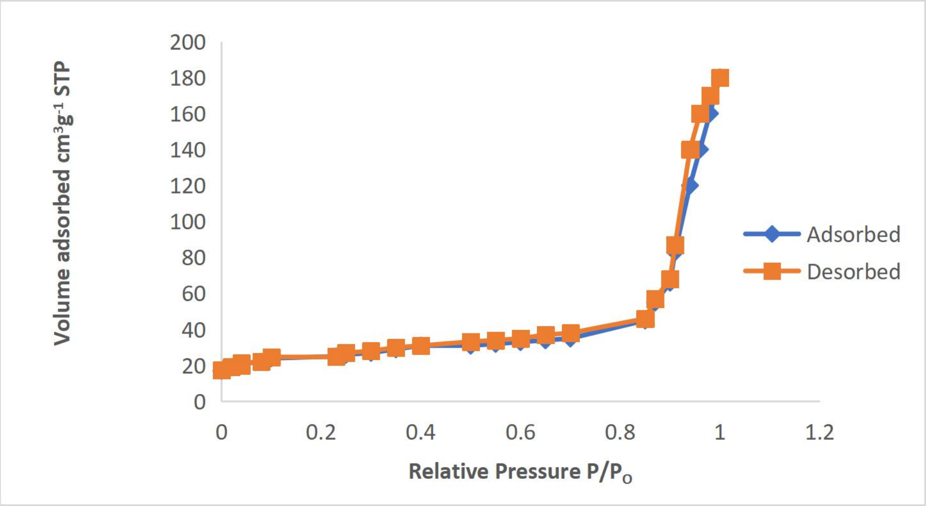

Fig 5(a): N_2 adsorption-desorption isotherms of *CAAgNP*

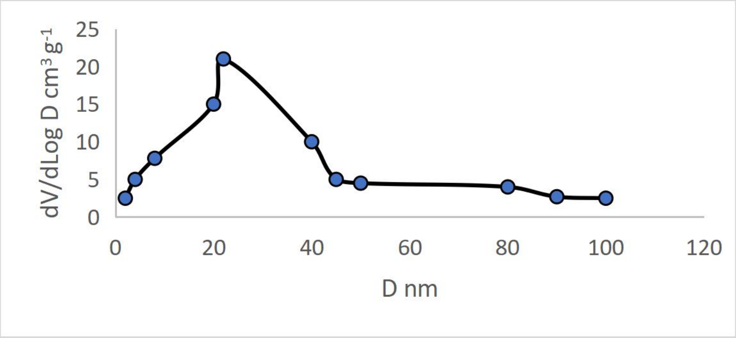

Fig 5(b) : BJH isotherms for *CA AgNP*

Corrosion inhibitory studies

Using CA dye and CA AgNP as an inhibitor, the effects of concentration and temperature on mild steel corrosion in 1 M HCl were examined at temperatures of 303k, 313k, 323k, and 333k. The findings are shown in Figs 6a and 6b. The results showed that the inhibitors reduced the metal sample's corrosion in the acid medium since the corrosion rate in the blank was higher than in the solution containing CA dye and CA AgNP inhibitor. It was discovered that the corrosion rate of the steel sample increased with temperature and decreased with an increase in CA dye and CA AgNP inhibitor concentrations [26]. In general, it has been shown that inhibitor concentrations and temperature have an impact on the rate at which mild steel corrodes [27].

The presence of crude dye and nanoparticles reduced the corrosion rates, implying that they actually retarded the mild steel corrosion due to the presence of heteroatoms and π-electron systems, which also suggest that they have a great propensity to adsorb on metal surfaces and other adsorbents [3] but the corrosion rate was less in the *Ag*-Nanoparticles dye than the crude dye at the same concentration. Similar trend has also been reported in literature [27].

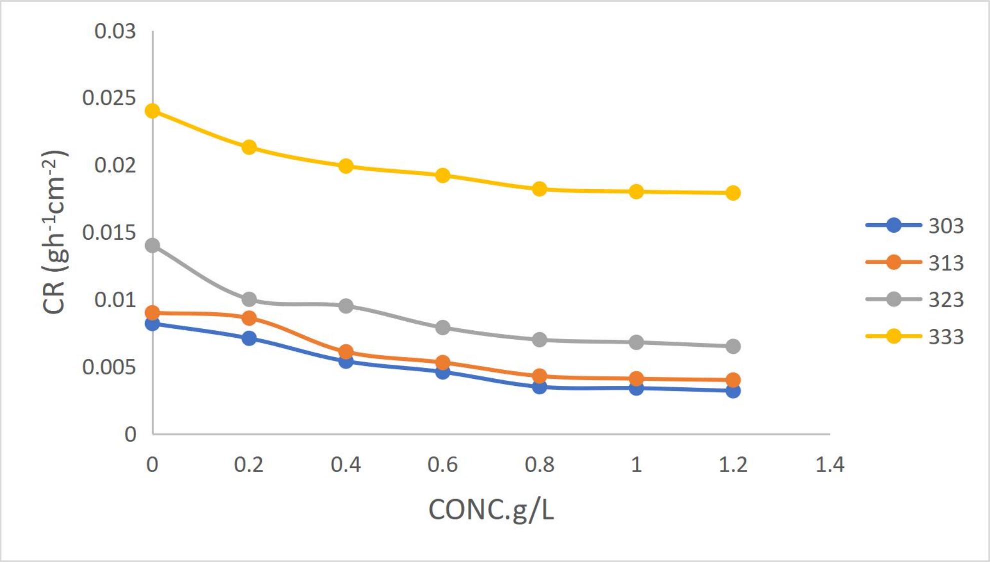

Fig. 6(a): Corrosion Rate of mild Steel in 1M HCL in presence and absence of CA dye

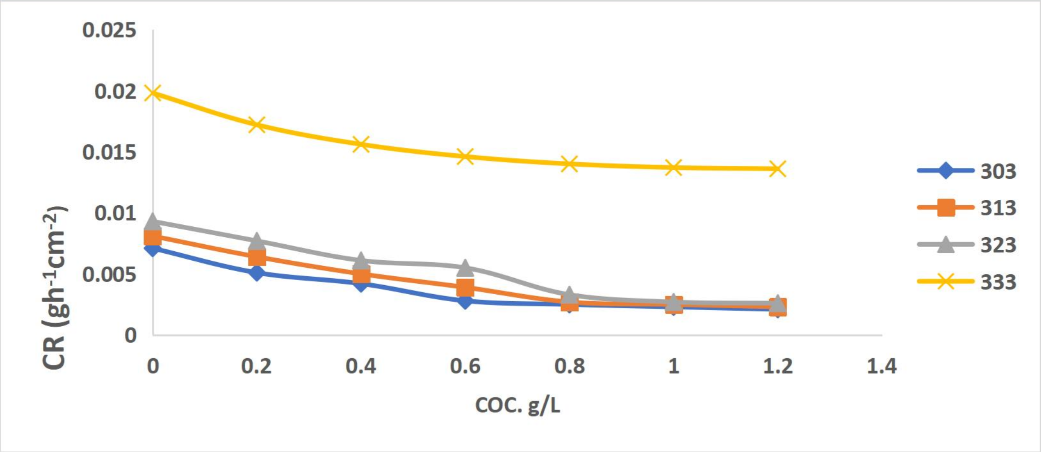

Fig. 6(b): Corrosion rate of mild steel in 1M HCL in presence and absence of CA AgNP

Inhibitor efficiency

The values of the inhibition efficiency (% IE) of the CA dye and CA AgNP inhibitor on the corrosion of the metal sample in acid solution are displayed in (Figs.7a and 7b). It was shown that the (%IE) decreased with rising temperatures and increased with increases in inhibitor concentration. As the temperature rises, the inhibitory efficiency actually decreases, suggesting that the extracts adsorb to the metal surface by a physical adsorption process [28]. This is in line with previous results found in the literature [4,29]. The decline in effectiveness of dye extracts and dye nanoparticles with temperature is typical of most inhibitors from plant biomass. It is thought that some of the phytochemicals included in the CA dye extract, such as tannins, flavonoids, alkaloids, and polyphenols, contribute to its efficacy. These molecules have heteroatoms (N, S, and O) that can bind to iron surface to create complexes that serve as a shield from ions that can cause corrosion. [30]. The efficacy of the dye extracts and dye nanoparticles rose as concentration increased, suggesting that increasing concentration may lead to improved inhibitory efficiency [4].

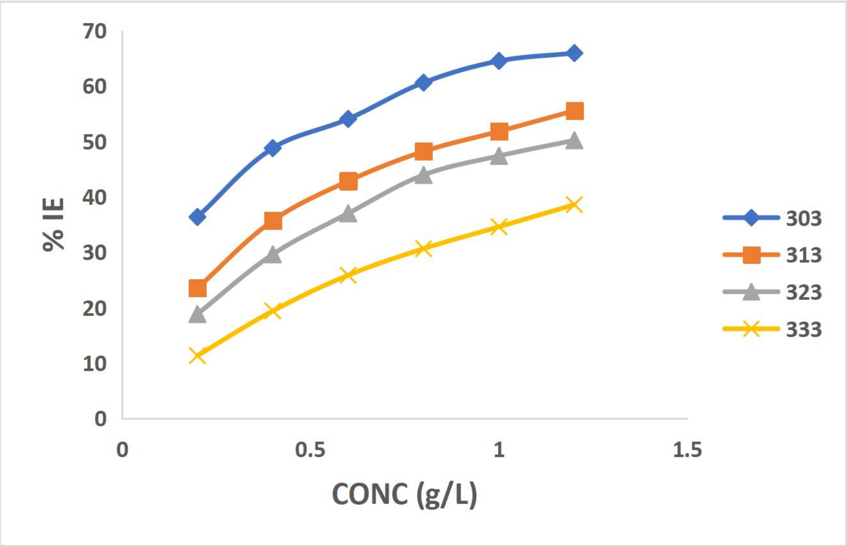

Fig 7(a): Inhibition efficiency of CA dye

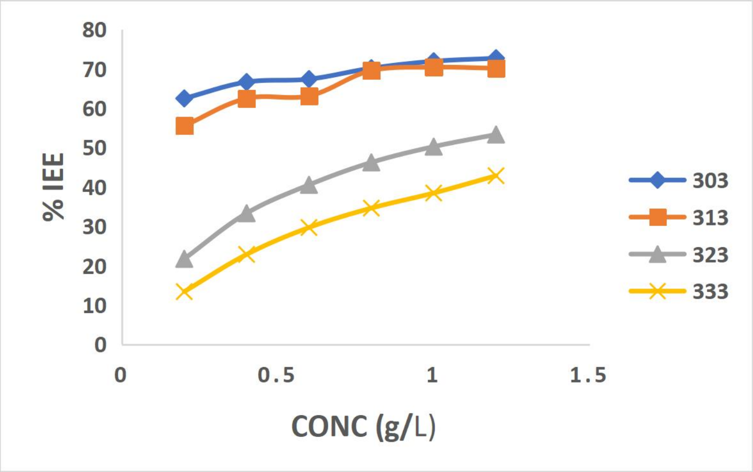

Fig. 7(b): Inhibition efficiency of CA AgNp

Thermodynamics studies

Using the Arrhenius equation Ln CR = - Ea / RT + ln A, the activation energy (Ea) for the dissolution of mild steel in 1.0 M HCl solution at different temperature values was determined with and without the addition of CA AgNp. Linear graphs were produced by the ln C against 1/T (Fig.8a). The slopes of each linear plot, which correspond to -Ea/RT, were used to derive the activation energy values for the process. In Table 2, the inhibited solutions exhibit higher activation energies compared to the uninhibited solution. The physical adsorption mechanism is indicated by the rise in apparent activation energy when the CA AgNp is present [31]. The larger energy barrier was the cause of the higher Ea values when an inhibitor was present. This finding implies that the increased energy barrier for the metal dissolution makes CA AgNp's corrosion inhibition viable [31]. Formation of thin film on the metal surface serves as a barrier to both energy and mass transfer, that raise the activation. Consequently, the outcome demonstrates that physical adsorption is the method of CA AgNp adsorption [32]. The trend of inhibition efficiency with temperature in this medium is consistent with the reduction in activation energy at high inhibitor concentrations [32].

Entropy and enthalpy of the transition stage, respectively. were ascertained from the plots of ln(CR/T) versus 1/T for the mild steel corrosion in 1.0 M HCl solution at various concentrations (Fig.9b). The slope (- ΔH*/ R) and intercept {ln(R /Nh)+ΔS*/ R} of the linear plots were used to calculate the enthalpy and entropy of activation, respectively. These values are shown in Table 2. The endothermic process yielded positive values for the transition state enthalpy ΔH*, which increased with concentration. This indicates that the dissolution of the metal in the presence of inhibitors is a sluggish process [33]. When the inhibitors are present or absent, the ΔS* values are negative. The mechanism of the hydrogen gas evolution reaction has apparently been linked to this negative entropy of activation. [20].

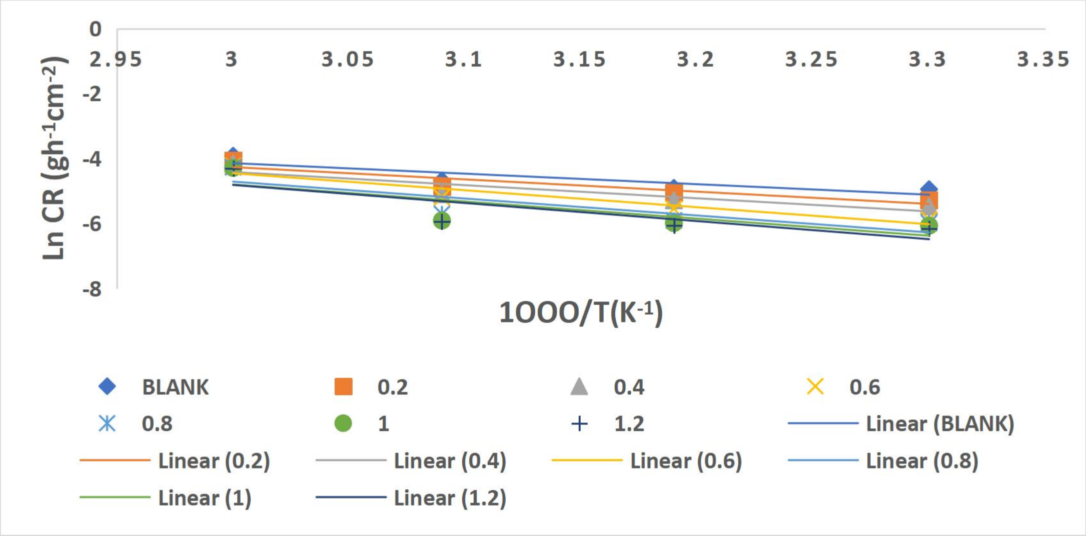

Fig. 8(a): Arrhenius plot for mild steel in 1M HCl in different concentration of CA AgNP and blank for weight loss methods

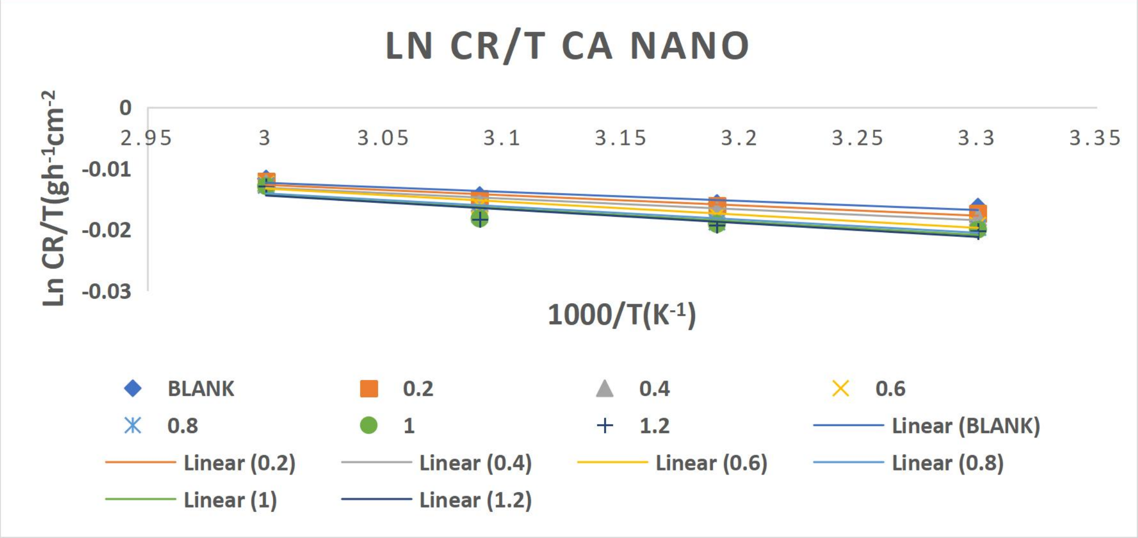

Fig. 8(b): Transition state plot for mild steel in 1M HCl in different concentration of CA AgNP and blank for weight loss method

Table 2: Thermodynamic activation parameters of corrosion inhibition of mild steel in 1.0 M HCl in the absence and presence of various concentrations of CA AgNP dye

Concentration (gL^{-1})	Activation energy E_a ($KJ mol^{-1}$)	Enthalpy ΔH^0 ($KJ mol^{-1}$)	Entropy ΔS^0 ($J mol^{-1}K^{-1}$)
Blank	27.52	25.01	-196.76
0.2	33.67	31.09	-188.20
0.4	36.33	33.67	-187.43
0.6	45.70	42.98	-184.78
0.8	47.70	45.17	-183.98
1.0	49.47	46.84	-183.46
1.2	51.75	49.05	-182.81

Adsorption Isotherm

The adsorption process free energy, ΔG^o_{ads} was calculated using the formula $\Delta G^o_{ads} = -RT \ln(55.5\times K_{ads})$. From the findings ΔG^o_{ads} have negative values which indicate that adsorption onto the steel surface appears to be a spontaneous process and the adsorption mechanism Physisorption. Physisorption is typically associated with the adsorption of free energy ($\Delta G^o < -40$ KJ/mol) [34].

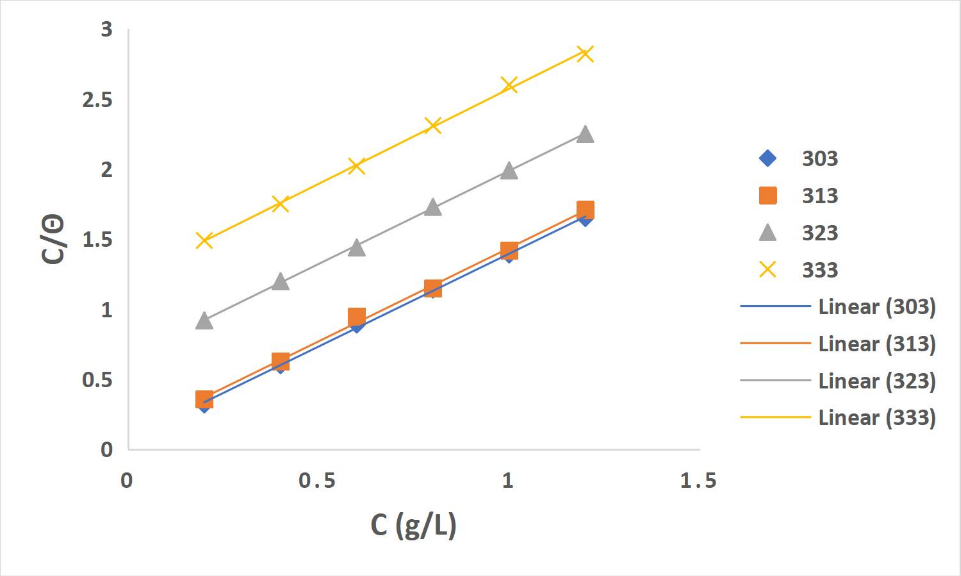

Fig. 9: Langmuir adsorption isotherms for mild steel in 1M HCl solution of CA AgNP at different concentrations by weight loss method

Table 3: Calculated parameters of Langmuir isotherm for the adsorption of CA AgNP in 1.0 M HCl at different temperatures

Temperature(k)	R^2	K_{ads}	Slope	ΔG^o_{ads}
303	0.978	5.319	1.07	-14.33KJ
313	0.960	4.505	1.08	-14.37KJ
323	0.980	2.000	1.64	-12.65KJ
333	0.994	1.307	1.71	-11.86KJ

Surface morphology analysis

In comparison to plain pristine mild steel (Fig. 11a), the SEM images of mild steel submerged in 1M HCl, CA dye, and CA AgNp inhibitor are displayed in (Figs. 11b, 11c, and 11d). When mild steel was submerged in 1M HCl Blank solution, considerable surface damage was seen (Fig. 11b), suggesting that the surface is heavily corroded. In the presence of 1.0 g/L of inhibitor, the mild steel's surface was shielded from visible surface morphology (Fig. 11c and 11d), and the smooth surface that resulted from the inhibitor's presence suggested limited corrosion. The data derived from the EDX measurement of iron weight concentration additionally demonstrates that the mild steel surface was protected by the inhibitor addition when 1.0 g/L of inhibitor was present. The mild steel surface was shielded from corrosion in the presence of CA and CA AgNp inhibitors, which is functioning as corrosion inhibitors in 1M HCl solution, according to the SEM pictures and EDX analysis. These outcomes compare favorably to those of other techniques, such as weight loss assessments.

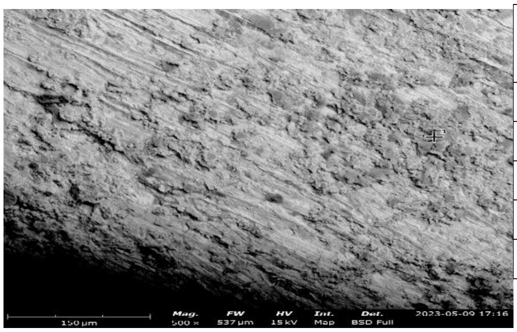

Element Number	Element Symbol	Element Name	Atomic Conc.	Weight Conc.
26	Fe	Iron	57.83	93.37
8	O	Oxygen	22.17	10.81
12	Mg	Magnesium	4.29	2.59
14	Si	Silicon	3.61	2.52
6	C	Carbon	1.71	0.51

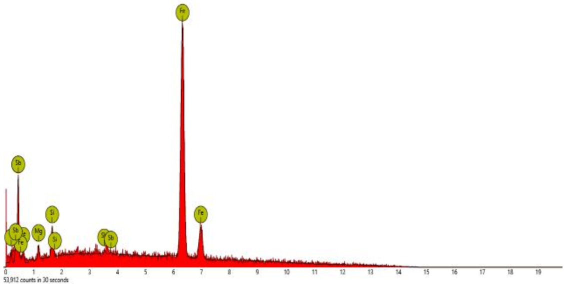

Fig 11(a):SEM image and EDX analysis of plain pristine mild steel

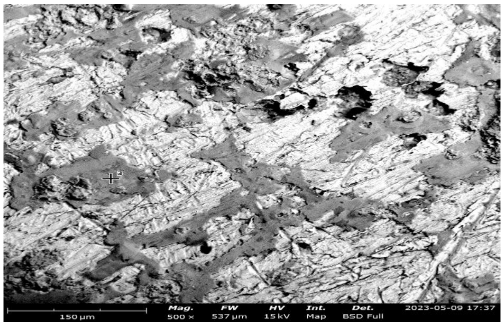

Element Number	Element Symbol	Element Name	Atomic Conc.	Weight Conc.
8	O	Oxygen	57.42	47.10
14	Si	Silicon	16.15	23.25
12	Mg	Magnesium	15.11	18.82
7	N	Nitrogen	7.96	5.72
6	C	Carbon	2.01	1.24
26	Fe	Iron	1.35	3.87

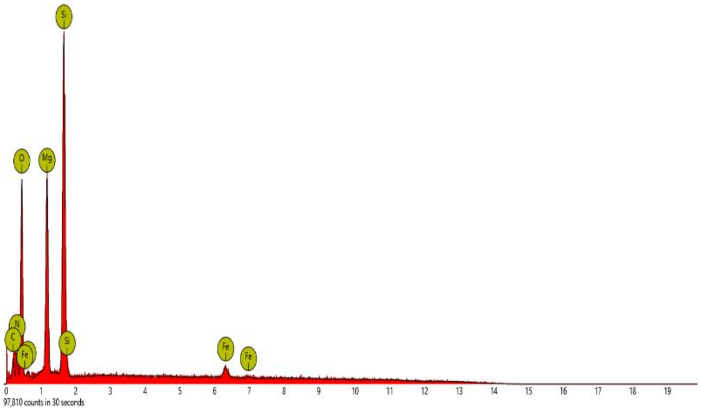

Fig11(b):SEM image and EDX analysis of mild steel after immersion in 1M HCl Blank solution

Element Number	Element Symbol	Element Name	Atomic Conc.	Weight Conc.
8	O	Oxygen	42.19	27.62
26	Fe	Iron	24.10	51.49
7	N	Nitrogen	7.72	4.14
12	Mg	Magnesium	4.27	3.97
14	Si	Silicon	3.50	3.76
6	C	Carbon	2.22	1.02

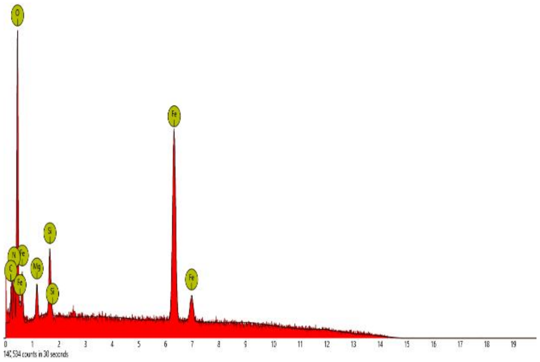

Fig11(c): SEM image and EDX analysis of Mild steel after immersion into *CA* dye inhibitor solution

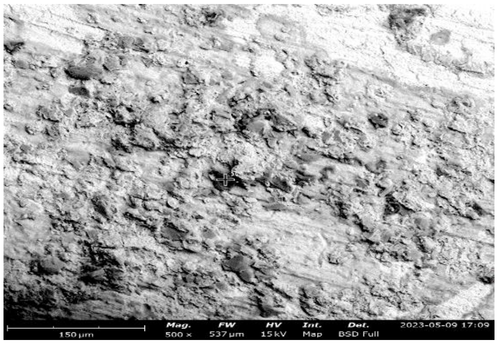

Element Number	Element Symbol	Element Name	Atomic Conc.	Weight Conc.
26	Fe	Iron	50.83	75.37
8	O	Oxygen	32.17	12.81
12	Mg	Magnesium	4.29	2.59
14	Si	Silicon	3.61	2.52
6	C	Carbon	1.71	0.51

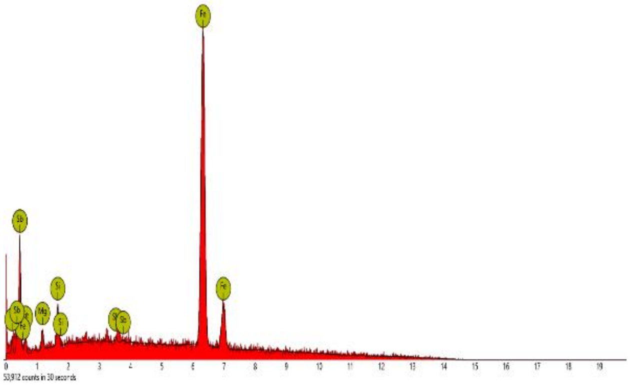

Fig11(c): SEM image and EDX analysis of Mild steel after immersion into *CA AgNP* inhibitor solution

Table 4: SEM-EDX parameters for mild steel corrosion in 1MHCl in the absence and presence of dye extracts and nnanoparticles

Samples	Weight Conc.	Difference In Weight Conc.	Percent. Difference in Weight Conc
Plain pristine Mild Steel	93.37	-	-
Mild Steel + 1M HCl	3.87	89.50	95.86
Mild Steel + *CA*	51.49	41.88	44.85
Mild Steel + *CA* AgNP	79.07	14.30	15.32

CONCLUSIONS

The study's findings demonstrate that *Cola acuminata* dye extract can be used as a reducing agent to create *Cola acuminata* silver nanoparticles, which can then be produced at a low cost and with minimal negative environmental impact. The resulting *Cola acuminata* silver nanoparticles can prevent mild steel from corroding in 1.0 M HCl. The mild steel sample's rate of corrosion rose with rising temperatures and fell with increasing *Cola acuminata* dye and *Cola acuminata* silver nanoparticle concentrations. It was found that the inhibition efficiency (%IE) rose as the inhibitor's concentration increased and fell with rising temperatures. The % inhibition efficiency and activation energy values increasing point to a physical adsorption mechanism. The inhibitor adsorbed endothermically on the metal surface, as indicated by the positive values of enthalpy and entropy of activation. The activation complex in the rate-determining step indicates associative mechanism. The *Cola acuminata* nanoparticles exhibited superior inhibition efficiency compared to the crude *Cola acuminata* dye extract, so *the Cola acuminata* nanoparticles can be used as an ecofriendly corrosion inhibitors in acidic medium.

REFERENCES

[1] Asafa ,T.B, Odusote, J.K, Ibrahim, O.S , Lateef, A, Durowoju, M.O, Azeez, M.A., Yekeen, T.A, Oladipo, I.C, Adebayo ,E.A, Badmus, J.A, Sanusi, Y.K. & Adedokun, O (2020). steel, stainless steel and aluminum in 1.0 M HCl medium *IOP Conf. Series: Materials Science and Engineering* 805, 1-17

[2] Ismail, A .(2016). A Review of green corrosion inhibitor for mild steel in Seawater, *ARPN Journal of Engineering and Applied Sciences* . 11(14), 8710-8714

[3] Peme, T., Olasunkanmi, L.O., Bahadur, I., Adekunle, S., Kabanda, M.M. & Ebenso, E.E. (2015). Adsorption and Corrosion Inhibition Studies of Some Selected Dyes as Corrosion Inhibitors for Mild Steel in Acidic Medium: Gravimetric, Electrochemical, Quantum Chemical Studies and Synergistic Effect with Iodide Ions, *Molecules*, 20 , 16004-16029.

[4] Godwin, A.I., Surma, N. & John, O.I. (2022). Ag-nanoparticles Mediated by *Lonchocarpus laxiflorus Stem Bark* Extract as Anticorrosion Additive for Mild Steel in 1.0 M HCl Solution, *Progress in Chemical and Biochemical Research* , 5(2),133-146

[5] Efe, M. O., Stephen, A. J. & Asefon, O. A. (2016). The Phytochemical Properties and Antimicrobial Potentials of Aqueous and Methanolic seed Extract of Cola nitida (Vent.) and *Cola acuminata* (Beauvoir) grown in South West, Nigeria Saudi J. Med. Pharm. Sci., 2 (12), 354-363

[6] Abdul-Rashid, I. M., Moses, M.S., Kabiru, H., Saviour, A. U. & Tawfik, A S. (2020). Evaluation of the corrosion inhibition efficacy of *Cola acuminata* extract for low carbon steel in simulated acid pickling environment , *Environ Sci Pollut. Res. Int .,* 27(27), 34270-34288.

[7] Taofeek, A. Y., Musibau, A. A, Akeem, A., Agbaje, L., Tesleem, B. A., Iyabo, C. O., Samuel O.O & Adewumi A. A (2017) Safety evaluation of green synthesized *Colanitida* pod, seed and seed shell extract-mediated silver nanoparticles (AgNPs) using an *Alliumcepa* assay, *Journal of Taibah University for Science*, 11(6), 895-909

[8] Pratap, R., Manthur, P., Ramchander, M., Rama, K., Veera, B.N. & Raju, N. (2014). Biogenic Synthesis of Silver Nanoparticles Using *Tectona grandis* Leaf Extract and evaluation of their Antibacterial Potential, *International Journal of ChemTech Research,* 6, (1) ,293-298.

[9] Khalid, S., Shahzad, A., Basharat, N., Abubakar, M. & Anwar, P. (2018). Phytochemical Screening and Analysis of Selected Medicinal Plants in Gujrat. *J Phytochemistry Biochem* 2, 108.

[10] Seema, K. & Jaya, M. (2020). Extraction, Phytochemicals Screening and Antibacterial activity of Carica papaya Leaf Extracts,*Der Pharma Chemica*, 12(5), 41-47.

[11] Olasehinde, E.F., Agbaffa, B.E. Adebayo, M.A. & Enis, J. (2022). Corrosion protection of mild steel in acidic medium by titanium-based nanocomposite of *Chromolaena odorata* leaf extract *Materials Chemistry and Physics*, 281,1-10

[12] Kanoma A. I., Muhammad, I., Abdullahi, S., Shehu, K., Maishanu, H. M.& Isah, A. D. (2014). Qualitative and Quantitative Phytochemical Screening of Cola Nuts (*Cola Nitida And Cola acuminata*) *Journal of Biology, Agriculture and Healthcare* ,4, (5),89

[13] Mabasa, X. E., Mathomu, L. M., Madala, N. E., Musie, E. M. & Sigid, M. T. (2021). , Molecular Spectroscopic (FTIR and UV-Vis) and Hyphenated Chromatographic (UHPLC TOF-MS) Analysis and In Vitro Bioactivities of the *Momordica balsamina* Leaf Extract. *Biochemistry Research International,* 2021, 1-12

[14] Patle, T. K., Shrivas, K., Kurrey, R., Upadhyay, S., Jangde, R. & Chauhan, R. (2020). Phytochemical screening and determination of phenolics and flavonoids in *Dillenia pentagyna* using UV-vis and FTIR spectroscopy, *Spectrochimica Acta Part A: Molecular and Biomolecular Spectroscopy*, 242.

[15] Sastry, M., Mayya, K. S. & Bandyopadhyay, K. (1997). pH Dependent changes in the optical properties of carboxylic acid derivatized silver colloidal particles. *Colloids Surf. A: Physicochem. & Engi. Aspects* 127, 22,1–228.

[16] Tiara, E. A., Windri, H. & Cuk, I. (2020). The UV-VIS Spectrum Analysis From Silver Nanoparticles Synthesized Using *Diospyros maritima*. Leaves Extract *Advances in Biological Sciences Research,*.14, 411-419

[17] Ahmed, S., Saifullah Ahmad, M., Swami, B.l. & Ikram, S. (2016). Green synthesis of silver nanoparticles using *Azadirachta indica* aqueous leaf extract. *Journal of Radiation Research and Applied Sciences;* 9(1), 1-7.

[18] Supraja, N., Kishore, B., Rajasekhar, K.K. & Padmavathamma, M. (2020). Synthesis of Carica Papaya (Leaf, Peel and Seed) Extracts Mediated Ag Nanoparticles for Industrial and Medical Applications *Chem. Sci. Eng. Res*, 2(5), 29-39.

[19] Emeka, E.E., Ojiefoh, O.C., Aleruchi, C., Hassan, L.A., Christiana , O.M., Rebecca, M., Dare, E.O. & Temitope, A.E. (2014) Evaluation of antibacterial activities of silver nanoparticles green-synthesized using pineapple leaf (*Ananas comosus*), *Micron* ,57, 1–5.

[20] Shankar, S., Jaiswal, L., Aparna, R.S.L. & Prasad, R.G.S.V. (2014). Synthesis , characterization, in vitro biocompatibility, and antimicrobial activity of gold, silver and gold silver alloy nanoparticles pre-pared from *Lansium domesticum* fruit peel extract, *Mater. Lett*.,137 ,75–78

[21] Agbaje, L, Musibau, A. A., Tesleem, B. A., Taofeek, A. Y., Akeem, A., Iyabo, C. O., Luqmon, A., Sadiat, E. A., Sunday, A. O., Evariste, B. G. & Lorika, S. B. (2016). Biogenic synthesis of silver nanoparticles using a pod extract of *Cola nitida*: Antibacterial and antioxidant activities and application as a paint additive, *Journal of Taibah University for Science,* 10, 551–562

[22] Rautela, A., Jyoti, R. & Mira, D. (2019). Green synthesis of silver nanoparticles from *Tectona grandis* seeds extract: characterization and mechanism of antimicrobial action on different microorganisms, *Journal of Analytical Science and Technology,* 10 (5).

[23] Merajuddin, K., Ponmurugan, K., Hamad, Z. A., Mufsir, K., Mujeeb, K., Syed, F. A. & Mohammed, R.S, (2022).Green Synthesis of Silver Nanoparticles Using *Juniperus procera* Extract: Their Characterization,and Biological Activity *Crystals*, 12, 420.

[24] Li, Z., Liu, D., Ca, Y., Wang, Y. & Teng, J. (2019). Adsorption pore structure and its fractal characteristics of coals by N_2 adsorption/desorption and FESEM image analyses, *Fuel* 257,116031

[25] Thommes, M., Kaneko, K., Neimark,A.V., Olivier, J.P., Rodriguez-Reinoso, F., Rouquerol, J. & Sing. K.S.W, (2015) Physisorption of gases, with special reference to the evaluation of surface area and pore size distribution (IUPAC Technical Report), *Pure Appl. Chem*. 87, 1051–1069

[26] Sanatkumar, B.S., Nayak, J. & Nityananda Shetty, A. (2012). Influence of 2-(4-chlorophenyl)-2-oxoethyl benzoate on the hydrogen evolution and corrosion inhibition of 18 Ni 250 grade weld aged maraging steel in 1.0 M sulfuric acid medium, *Int. J. Hydrogen Energy*, 37, 9431–9442,

[27] Odewunmi, N.A, Umoren, S.A. & Gasem, Z.M. (2015). Watermelon waste products as green corrosion inhibitors for mild steel in HCl solution.„*J. Environ. Chem. Eng.* 3(1) , 286-296.

[28] Oguzie, E. E. (2006). Studies on the inhibitive effect of *Occimum viridis* extract on the acid corrosion of mild steel," *Journal of Materials chemistry and physics*, 99, (2-3) , 441–446

[29] Egbeneje, V.O., Okhale, S .E., Moisi, C, Ogbogo, I.O. & Ojo, O. (2023). Evaluation of the Inhibitive Properties of Silver Nanoparticles in *Senna occidentalis* Root Extract as Corrosion Inhibitor of Mild Steel, *Tanzania Journal of Science* 49(3), 655-663

[30] Kandregula, C., Chinthakuntla, A., Rao, K. & Rajendar, V. (2014). Green synthesis of TiO_2 nanoparticles using Hibiscus flower extract, *Int. Conf. Emerg. Technol. Mech*. Sci. 2, 79–82.

[31] Umoren, S.A. & Solomon, M.M. (2015). Performance assessment of poly (methacrylic acid)/ silver nanoparticles composite as corrosion inhibitor for aluminium in acidic environment, *J. Adhes.Sci.Technol*., 9, 2311–2333,

[32] Eddy, N.O. & Ebenso, E.E (2008). Adsorption and inhibitive properties of ethanol extract of *Musa sapientum* peels as a green corrosion inhibitor for mild steel in H_2SO_4. *Afr. J. Pure Appl. Chem*. 2(6), 46-54.

[33] Liu, Y., Miao, J., Han, H. & Xu, P. (2021). Differences in influence of particle size on the adsorption capacity between deformed and undeformed coal, *ACS Omega 6* , 5886–5897.

[34] Muthukrishnan, P., Jeyaprabha, B. & Prakash, P. (2017). Adsorption and corrosion inhibiting behavior of *Lannea coromandelica* leaf extract on mild steel corrosion, *Arab. J. Chem*., 10, 2343–2354